OXFORD

Cerebral Cortex, 2023, **33**, 5808–5816
https://doi.org/10.1093/cercor/bhac461
Advance access publication date 28 November 2022
Original Article

TDP-43 knockdown in mouse model of ALS leads to dsRNA deposition, gliosis, and neurodegeneration in the spinal cord

Ryan A. Milstead [1,2], Christopher D. Link[1], Zuoshang Xu[3], Charles A. Hoeffer [1,2,4,*]

[1]Department of Integrative Physiology, University of Colorado, Boulder, Boulder CO 80303,
[2]Institute for Behavioral Genetics, University of Colorado, Boulder, Boulder, CO 80303,
[3]Department of Biochemistry and Molecular Biotechnology, University of Massachusetts Chan Medical School, Worcester, MA, 01655,
[4]Linda Crnic Institute, Anschutz Medical Center, Aurora, CO 80217

*Corresponding author: Institute for Behavioral Genetics, University of Colorado, 1480 30th Street, Boulder, CO 80303, USA. Email: Charles.Hoeffer@colorado.edu

Transactive response DNA binding protein 43 kilodaltons (TDP-43) is a DNA and RNA binding protein associated with severe neurodegenerative diseases such as amyotrophic lateral sclerosis (ALS), primarily affecting motor neurons in the brain and spinal cord. Partial knockdown of TDP-43 expression in a mouse model (the amiR-TDP-43 mice) leads to progressive, age-related motor dysfunction, as observed in ALS patients. Work in *Caenorhabditis elegans* suggests that TDP-43 dysfunction can lead to deficits in chromatin processing and double-stranded RNA (dsRNA) accumulation, potentially activating the innate immune system and promoting neuroinflammation. To test this hypothesis, we used immunostaining to investigate dsRNA accumulation and other signs of CNS pathology in the spinal cords of amiR-TDP-43 mice. Compared with wild-type controls, TDP-43 knockdown animals show increases in dsRNA deposition in the dorsal and ventral horns of the spinal cord. Additionally, animals with heavy dsRNA expression show markedly increased levels of astrogliosis and microgliosis. Interestingly, areas of high dsRNA expression and microgliosis overlap with regions of heavy neurodegeneration, indicating that activated microglia could contribute to the degeneration of spinal cord neurons. This study suggests that loss of TDP-43 function could contribute to neuropathology by increasing dsRNA deposition and subsequent innate immune system activation.

Key words: ALS; double-stranded RNA; immunostaining; neuropathology; TDP-43.

Introduction

Frontotemporal Dementia (FTD) and Amyotrophic Lateral Sclerosis (ALS) are believed to share a similar etiology because both involve pathology associated with TDP-43 (Kwong et al. 2007). TDP-43 is a DNA and RNA binding protein found in nearly every cell of the body, but it is directly related to neurodegenerative diseases specific to the CNS. TDP-43 plays a role in almost every aspect of RNA maintenance, including production, splicing, transport, and metabolism (Buratti and Baralle 2001; van Blitterswijk and Landers 2010). In support of TDP-43 being a critical aspect of FTD/ALS pathology, a small percentage of familial ALS cases are associated with the inheritance of mutations in the gene encoding TPD-43 (Sreedharan et al. 2008).

Previous studies using the *Caenorhabditis elegans* model and TDP-43 ortholog, TDP-1, show associations between TDP-1, chromatin processing, and double-stranded RNA (dsRNA) accumulation (Saldi et al. 2014, 2018). dsRNA accumulation is thought to contribute to the cellular toxicity observed in a mouse model of ALS/FTD based on AAV transfection-driven expression of poly proline-arginine dipeptides that are a product of the *C9orf72* hexanucleotide expansion (Zhang et al. 2019). We have previously shown that TDP-43 knockdown (KD) in primary rat astrocytes leads to immune system activation through the production of dsRNA and protein kinase R (PKR) (LaRocca et al. 2019). TDP-43 depletion in SH-SY5Y neuroblastoma has also been shown to induce dsRNA accumulation (Shelkovnikova et al. 2018), and TDP-43 knockdown in HEK293 cells leads to the accumulation of endogenous dsRNA that can trigger a lethal immune response mediated by interferon signaling and RIG-I-like receptors (Dunker et al. 2021).

Given TDP-43's known associations with FTD and ALS, mouse models of TDP-43 dysfunction could be a promising target for investigating neurodegenerative pathology. One such model, amiR-TDP43, was created using constitutively expressed artificial micro-RNA (amiRNA) against TDP-43 mRNA (amiR-TDP43). This miRNA expression leads to a partial loss of function and age-related motor dysfunction such as human ALS (Yang et al. 2014). Interestingly, TDP-43 KD occurs mainly in astrocytes in this model of ALS. Still, signs of cortical and spinal neurodegeneration are rampant, indicating an essential role for astrocytes and neurons in the associated pathologies.

Here, we use immunostaining to show that TDP-43 KD via amiR-TDP43 leads to a wide variety of pathological phenotypes and affects multiple neural cell types in the spinal cord. We observed dsRNA accumulation associated with increased astrogliosis, microgliosis, oligodendrocyte marker expression differences, and neurodegeneration in the spinal cord compared with wild-type (WT) controls. This study provides evidence for a possible pathway for ALS and FTD pathology involving TDP-43, dsRNA, and the innate immune system.

Received: August 12, 2022. **Revised:** October 28, 2022. **Accepted:** October 29, 2022

Materials and methods

Mice

All animal procedures were reviewed and approved by the Institutional Animal Care and Use Committee of the University of Colorado, Boulder.

Artificial micro-RNA targeting TDP-43 (amiR-TDP43) was designed and constructed as described in Yang et al. (2010) and Yang et al. (2011). amiR-TDP-43 mice were generated using the pronuclear injection method leading to constitutively expressed amiR-TDP43. The amiR-TDP43 reduces TDP-43 expression without causing full-body knockout (KO) (Yang et al. 2014). The preinduction parent transgenic line (amiR–TDP43u or CAG-loxp-EGFP/3xpA-loxp-RFP-amiR-TDP43 mice) is available from the Jackson Laboratory as stock no. 017919. The post-induction line (amiR–TDP43i mice) is available from the Jackson Laboratory as stock no. 017934 and was used in this study.

Mouse spinal cord immunostaining

amiR-TDP43 and WT mice were fixed by transcardial perfusion using 4% paraformaldehyde (PFA) in PBS and post-fixed in the same fixative for 24–48 hrs. A segment of the lumbar spinal cord was dissected, soaked in PBS overnight, and then transferred to PBS containing 30% sucrose for 24 h at 4 °C for cryoprotection. Once cryoprotected, lumbar spinal cords were frozen using dry ice and Optimal Cutting Temperature compound and sectioned transversely at 30 μm on a cryostat (Leica). Spinal cord sections were stored in a cryoprotectant solution (30% sucrose and 30% ethylene glycol in phosphate-buffered solution) at −20 °C until being used for immunostaining. Lumbar spinal cord slices were washed using PBS-T (0.03% TritonX-100 in 1X PBS) and blocked for 1 h at 4 °C using a staining buffer (0.05 M Tris pH 7.4, 0.9% NaCl, 0.25% gelatin, 0.5% TritonX-100) with 2% donkey serum. After blocking, slices were incubated for 24–72 hrs with primary antibodies against NeuN (1:1000, Novus, NBP1–92693), K1/dsRNA (1:250, SCICONS, 10020200), Iba1 (1:250, Synaptic Systems, 234,004), GFAP (1:1000, PhosphoSolutions, 621-GFAP), OLIG2 (1:1000, Novus, NBP1–28667), TDP-43 (1:500, ProteinTech, 10,782–2-AP), ChAT (1:250, AB144P), or RFP (1:250, Rockland, 600–401-3795) diluted in the same blocking buffer mixture. Following primary antibody treatment, slices were washed in PBS-T and incubated in the dark at RT for 2 hrs with a combination of Hoechst dye (1:3000, ThermoFisher), Alexa Fluor 488-conjugated anti-mouse IgG2A (1:500, Invitrogen), Cy3-conjugated anti-guinea pig, anti-rabbit, or anti-goat (1:500, Jackson ImmunoResearch), Alexa Fluor 647-conjugated anti-mouse IgG2B (1:500, Invitrogen), or Cy5-conjugated anti-chicken or anti-rabbit (1:500, Jackson ImmunoResearch) secondary antibodies in staining buffer without donkey serum. After more PBS-T washes, slices were mounted on glass slides and coverslipped using Mowiol mounting compound. Z-stacks of the highest intensity third (10-μm thickness) of the lumbar spinal cord slices were imaged with a Nikon A1R Laser Scanning Confocal microscope, and 488 and 555 laser channels were imaged independently to confirm no crosstalk between secondary antibodies. Control tests with no primary or secondary antibodies were performed to confirm no remaining RFP fluorescence. All laser powers and detector gains were consistent between slices from the same experiment.

Mouse spinal cord immunostaining density quantification

Images were maximum-intensity projected across the z-stack to yield one image representing the entire thickness. For each image, a region of interest (ROI) was created containing both the dorsal and ventral horns in each hemisphere of the spinal cord (gray matter), with the peripheral edges of the slices excluded. Example ROIs are provided in each figure. After ROI creation, contrast adjustments were applied. The maximum contrast was kept consistent between all images for each experiment, and minimum contrast was set to the apex of the contrast histogram for each image to help reduce background interference. RGB images were exported, and ROIs were re-applied. This was done to remove the background signal while keeping the punctate intensity at a consistent level across all images, which facilitated proper quantification. Color channel intensities were summed and divided by ROI area (to account for variance in ROI sizes), yielding staining density. Density measurements were averaged for each animal within experiments, and TDP-43 KD animals were individually compared with the average of all WT measurements. Data were obtained from >3 images for each animal and each experiment.

Statistics

Statistics and graphs were generated using GraphPad Prism 9. All WT density measurements were combined for K1 dsRNA density quantifications (Fig. 2) to yield an average WT staining density. The average of each KD animal's density measurements was compared with the average of the WT density using a one-way ANOVA and Dunnett's multiple comparison test. For WT vs. KD analyses (all other figures), all WT and all KD values were averaged, and a two-tailed independent *t*-test was used to compare the means of both groups.

Results

TDP-43 knockdown leads to neurodegeneration

TDP-43 KD mice are known to have age-dependent motor dysfunction and cortical neurodegeneration (Yang et al. 2014). Because NeuN immunostaining has been used as a proxy for neurodegeneration in TDP-43-related neurodegenerative diseases (Yousef et al. 2017), we measured NeuN expression in the lumbar spinal cords of amiR-TDP43 mice compared with WT controls. Like the cortex, evidence for neurodegeneration was pronounced, including both decreased NeuN signal in neurons and decreased number of visible neurons (Fig. 1). Compared with WT controls, amiR-TDP43 mice have decreased NeuN expression in all visible cellular compartments (Fig. 1, 60×), with some animals showing regions of completely degenerated neurons with little to no visible NeuN stain.

TDP-43 KD leads to variably increased dsRNA expression in neurons

We immunostained for dsRNA within the spinal cords of amiR-TDP43 mice using the K1 antibody. K1 recognizes any dsRNA that has a helix longer than 40 base pairs, regardless of the sequence composition, by recognizing the A-form helix of dsRNA complexes (Schönborn et al. 1991). We found that TDP-43 KD spinal cords showed a variety of histological phenotypes, ranging from slight to very heavy deposition of dsRNA accumulation compared with WT controls (Fig. 2), with average dsRNA accumulation in the amiR-TDP43 mice higher than WT mice overall (Fig. 3). In general, dsRNA expression was limited to the dorsal and ventral horns of the spinal cord (gray matter). Neurodegeneration measured in Fig. 1 was especially evident in areas of dsRNA expression, with some animals showing both seemingly normal regions of NeuN expression and extensively degenerated regions. Given the

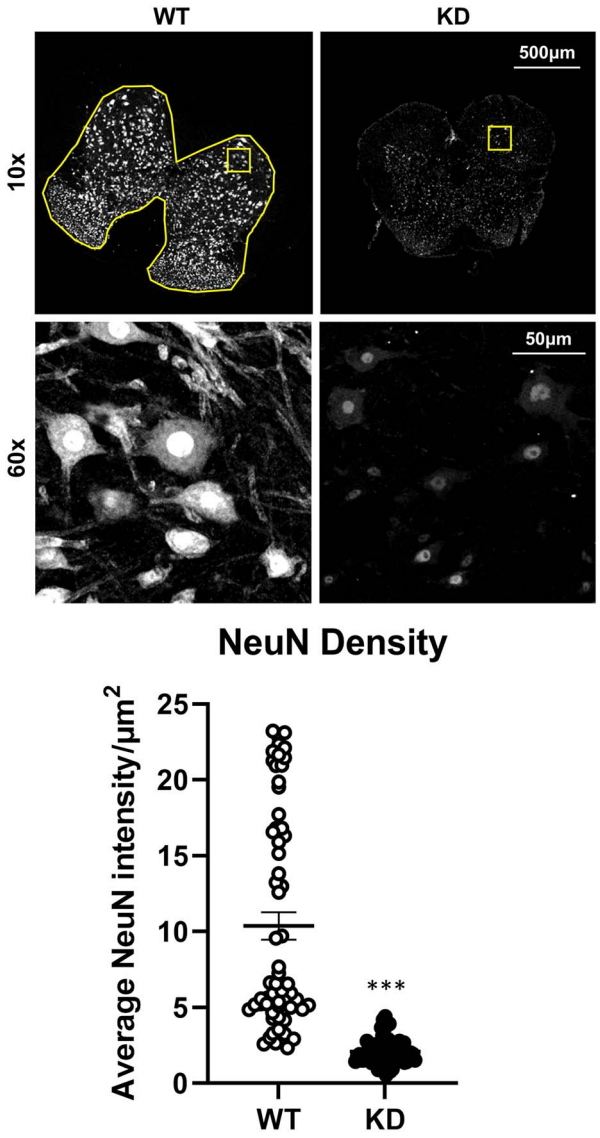

Fig. 1. amiR-TDP-43 (TDP43 KD) leads to decreased NeuN staining density within the gray matter of the lumbar spinal cord compared with WT controls. Average NeuN density in all quantified images from WT ($N = 6$, $n = 62$) and amiR-TDP-43 (TDP43 knockdown, KD) mice ($N = 5$, $n = 67$; N is the number of biological replicates, n is the total number of slices imaged from all biological replicates, minimum of 5 slices from a single N). Yellow boxes highlight 60× inset images; an example ROI is shown in yellow on WT 10×. Individual data points are plotted with mean and SEM. Two-tailed unpaired t-test shows a significant difference at $P < 0.0001$ (***).

proposed role of immune activity and neurodegeneration, we were also interested in what cell types are responsible for the increase in dsRNA. Therefore, we stained for K1 in conjunction with Iba1 (microglial marker) and NeuN (neuronal marker). Interestingly, dsRNA was found in neurons (indicated by dsRNA/NeuN costaining) but not in microglia (Fig. 3). We note that the dsRNA accumulation in neurons was largely cytoplasmic.

TDP-43 KD leads to large increases in both astro- and microgliosis

Reactive astrogliosis is a hallmark of nearly every CNS disorder, infection, and injury (Zamanian et al. 2012). Glial fibrillary acidic protein (GFAP) is a structural filament found within astrocytes that serves as a marker for reactive astrogliosis because of its responsiveness to CNS insults (Zamanian et al. 2012). During reactive astrogliosis, GFAP is upregulated, mirroring an increase in both astrocyte number and size. In response to TDP-43 KD, GFAP was highly induced in the gray matter compared with WT controls (Fig. 4a). Interestingly, in conjunction with increased GFAP expression and astrocyte number, TDP-43 KD animals showed an increase in oligodendrocyte transcription factor (OLIG2) expression along with a change from the normal nuclear expression pattern (Fig. 4b). The translocation of OLIG2 from the nucleus to the cytoplasm is a known hallmark of reactive astrocytes activated by inflammation (Cassiani-Ingoni et al. 2006). Like reactive astrogliosis, microglia respond to CNS insults in a similar manner, but their structural changes are much more dramatic. Resting microglia have a structure like astrocytes but with fewer processes that have more arborization (branching). When activated, microglia can revert to their macrophage origins, becoming what is known as "amoeboid" microglia (Woodburn et al. 2021). Compared with WT controls that showed normal, resting microglia, TDP-43 KD animals showed highly increased levels of Iba1 with a corresponding change in microglial morphology associated with immune activation (Fig. 4c).

TDP-43 KD leads to decreased TDP-43 expression, especially in regions of dsRNA

Expanding upon the results of Yang et al. 2014, we also immunostained for TDP-43 in the lumbar spinal cords of amiR-TDP43 mice. We found that TDP-43 KD spinal cords showed significantly decreased TDP-43 density in the gray matter of the spinal cords compared with WT controls (Fig. 5). TDP-43 KD animals with large deposits of dsRNA showed the largest decrease in TDP-43 compared with the large healthy neurons that showed intense TDP-43 stain in WT mice with no detectable K1+ dsRNA staining. K1+ cells in high K1 TDP-43 KD animals show little to no detectable cytoplasmic TDP-43 staining, and they also show degenerated nuclei, suggesting they could be dead or degenerating neurons, based on morphology and spinal location (though we cannot completely rule out the possibility they are other cell types) (Fig. 5, white arrows). These dead or dying neurons could explain the significant decrease in TDP-43 that we observed, while Yang et al. 2014 showed more modest reductions. Additionally, while the cytoplasmic depletion of TDP-43 is apparent in the neurons of TDP43 KD animals, there is little to no visible decrease in nuclear TDP-43. To confirm expression of the amiR-TDP43 transgene, we immunostained for the RFP marker included in this transgenic construct (the intrinsic fluorescence of RFP has been lost in these archival samples). We also probed for choline acetyltransferase (ChAT) to determine if dsRNA accumulation was occurring in motor neurons. While increased dsRNA was observed in ChAT+ neurons compared with WT controls, the RFP expression within motor neurons was minimal compared with surrounding glial cells (Fig. 6). This aligns with the results of Yang et al. 2014 who observed the largest TDP43 reduction in astrocytes.

Discussion

This study has provided new in vivo evidence for a possible role for dsRNA and immune activation in the neurodegeneration in TDP-43 proteinopathies like ALS and FTD. We show that knocking down TDP-43 function via an artificial miRNA leads to a myriad of histological changes in the spinal cord, including increased neuronal dsRNA accumulation, astrogliosis, microgliosis, increases in oligodendrocyte marker expression, and neurodegeneration. This study extends our work in *C. elegans* and primary cell

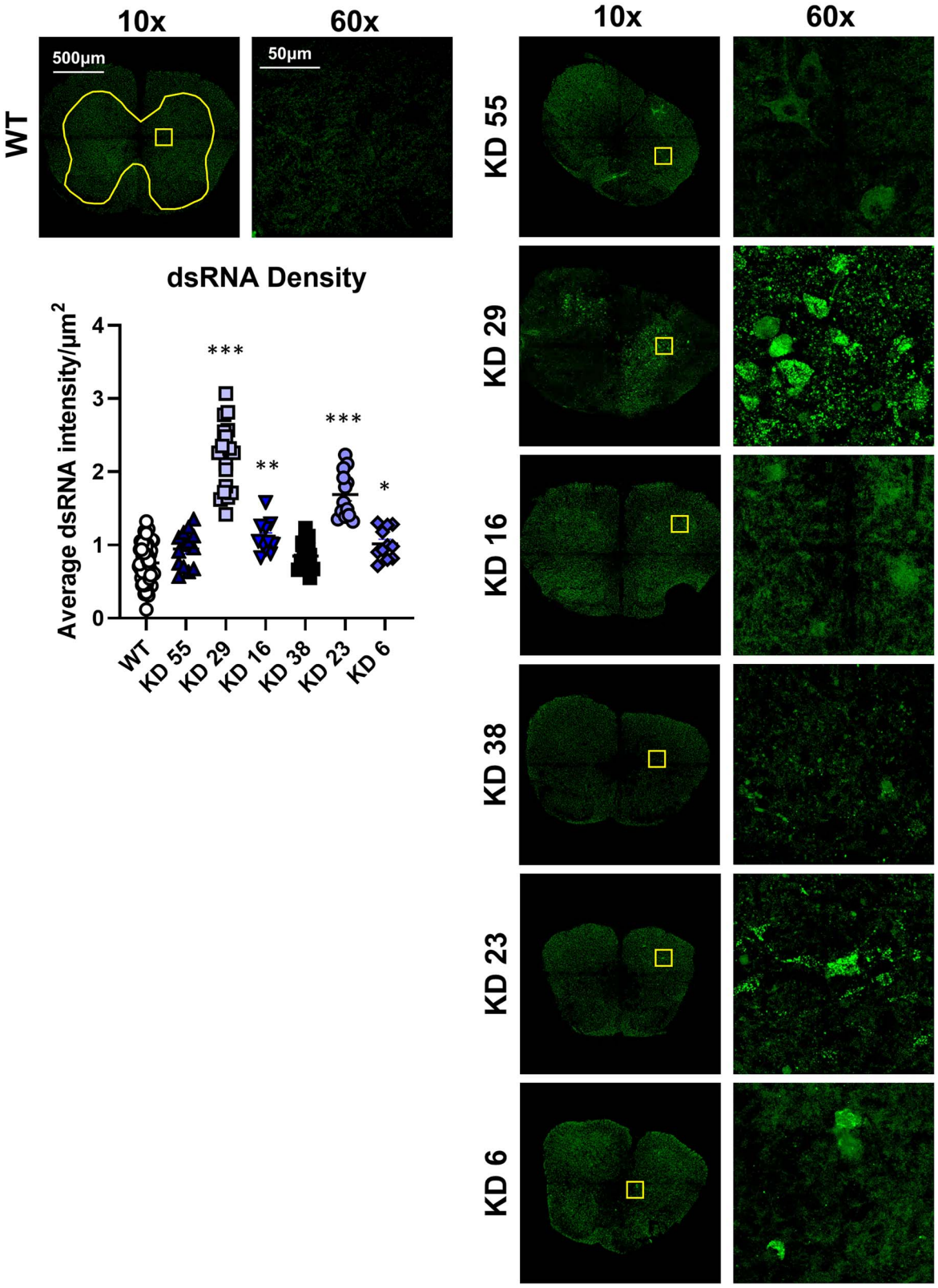

Fig. 2. TDP43 KD leads to variable increases in dsRNA deposition within the gray matter of the lumbar spinal cord compared with WT controls. Yellow boxes highlight 60× inset images; an example ROI for quantification is shown in yellow on the WT image. Individual data points are plotted with mean and SEM. KD# labels refer to individual amiR-TDP43 mice, ordered by age. One-way ANOVA *P*-value < 0.0001, Dunnett's multiple comparisons tests against WT controls show significance (* < 0.05, ** < 0.01, *** < 0.0001) for most but not all KD animals. ~12 images were quantified from each KD animal, and 65 total images from 5 animals were quantified for WT, 12–14 images per animal.

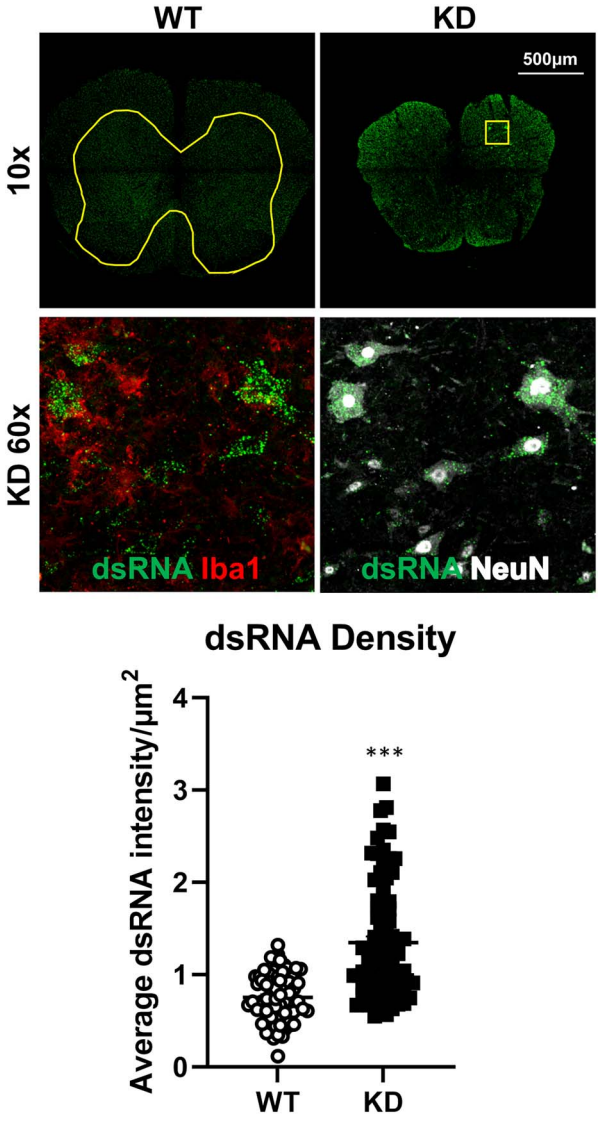

Fig. 3. TDP43 KD spinal cords show significantly higher dsRNA than WT controls found in neurons within areas of high microglial activation. Average dsRNA density in all quantified images from WT ($N = 5$, $n = 65$, 11–15 n per N) and TDP43 KD mice ($N = 6$, $n = 85$, 11–19 n per N). dsRNA shows overlap with NeuN in areas of microgliosis. Yellow boxes highlight 60× inset images; an example ROI is shown in yellow on WT 10×. Individual data points are plotted with mean and SEM. Two-tailed unpaired t-test shows a significant difference at $P < 0.0001$ (***).

culture, investigating the effects of TDP-43 depletion on an in vivo ALS model, adding a potential translational link between animal models and ALS/FTD patient pathologies. Although this study is limited by tissue availability, our results show that dsRNA accumulation is associated with a global reduction in TDP-43 in vivo.

dsRNA accumulation and the histopathologies measured in this study did not correlate well with age at death or details of paralysis (e.g., hind limb vs. total paralysis) (Table 1). The inability to identify correlations may be due to our limited sample size and the significant phenotypic variation of the amiR-TDP-43 mice. Nevertheless, the distribution of dsRNA accumulation in the spinal cord sections aligned with gliosis and neurodegeneration, and any amount of cytoplasmic dsRNA could be sufficient to induce an innate immune response and subsequent neurodegeneration. Another study from the Albers lab using AAV vectors to introduce sense and antisense GFP RNA into the olfactory sensory neurons of mice showed that cytoplasmic dsRNA was sufficient to induce neuronal cell death in vivo (Rodriguez et al. 2021). They also observed cytoplasmic dsRNA in the brains of ALS/FTD patients with the *C9ORF72* intronic nucleotide expansion. RT-PCR was used to demonstrate that this dsRNA included sequences from the C9ORF72 G_4C_2 -containing intron, although the possibility that other RNA transcripts contributed to this dsRNA was not investigated. Additionally, these patients showed increased cytoplasmic levels of TDP-43 inclusions, a classical hallmark of ALS and FTD pathology (Rodriguez et al. 2021).

To our knowledge, no rodent model of ALS has been examined for the deposition of dsRNA. While transgenic TDP-43 overexpression models might not be expected to replicate our observations in the amiR-TDP43 knockdown model, TDP-43 knock-in models should be more relevant, although in general, these models do not show the motor defects or TDP-43 cytoplasmic relocalization that are hallmarks of ALS (Stribl et al. 2014; White et al. 2018; Watanabe et al. 2020). One exception is the N390D/+ TDP-43 knock-in model of Huang et al. 2020, which is reported to replicate these hallmarks. We hope our study will encourage an examination of dsRNA deposition across the range of extant TDP-43 models, which will help determine the relationships between TDP-43 expression, gliosis, and dsRNA accumulation.

Our RFP staining results show that TDP43 KD in the amiR-TDP43 line occurs primarily in glial cells, a result originally reported by Yang et al. 2014. However, we observed the most robust K1 dsRNA staining in ChAT+ motor neurons and saw little evidence of glial dsRNA. These data suggest a more complex model in which glial cell TDP-43 reduction promotes neuronal dsRNA deposition leading to neurodegeneration and increased pathological marker expression we observed, as opposed to cell-autonomous effects of TDP-43 loss in neurons and subsequent dsRNA deposition. Using the Cre- loxP system, Peng et al. removed the gene for TDP-43 in GFAP-producing cells. These TDP-43 negative astrocytes showed transcriptomes similar to those of A1-reactive astrocytes, a neurodegenerative subtype of reactive astrocytes triggered by activated microglia, and similar to the amiR-TDP43 line, the animals developed motor deficits (Peng et al. 2020). Utilizing cell-type specific TDP-43 KD, future work could better identify contributing glial cell types and their mechanistic roles in dsRNA deposition.

Abnormal cytoplasmic deposition and nuclear depletion of TDP-43 are observed in ~97% of all ALS cases and a significant fraction of Alzheimer's disease (AD) and FTD cases (Amador-Ortiz et al. 2007; Josephs et al. 2014; Ling et al. 2015). This shuttling of TDP-43 from the nucleus to the cytoplasm could indicate loss of regular TDP-43 function and TDP-43 loss-of-function molecular phenotypes initially identified in model systems (Ling et al. 2015; Klim et al. 2019), such as RNA splicing alterations and inclusion of cryptic exons, have been validated in human patient samples (Chiang et al. 2010; Sun et al. 2017). These cryptic exons and splicing alterations could be the source of the observed dsRNA. Because of its role as an RNA-binding protein, TDP-43 dysfunction could be the link between these splicing errors, dsRNA production and accumulation, and subsequent neurodegeneration.

While dsRNA has been observed in the brains of patients with ALS/FTD with the *C9ORF72* expansion, many other neurodegenerative diseases are known as TDP-43 proteinopathies. Cytoplasmic inclusions of TDP-43 are common in diseases with different etiologies: primarily neurodegenerative diseases, including late-onset AD, Huntington's disease, and ALS/FTD; developmental

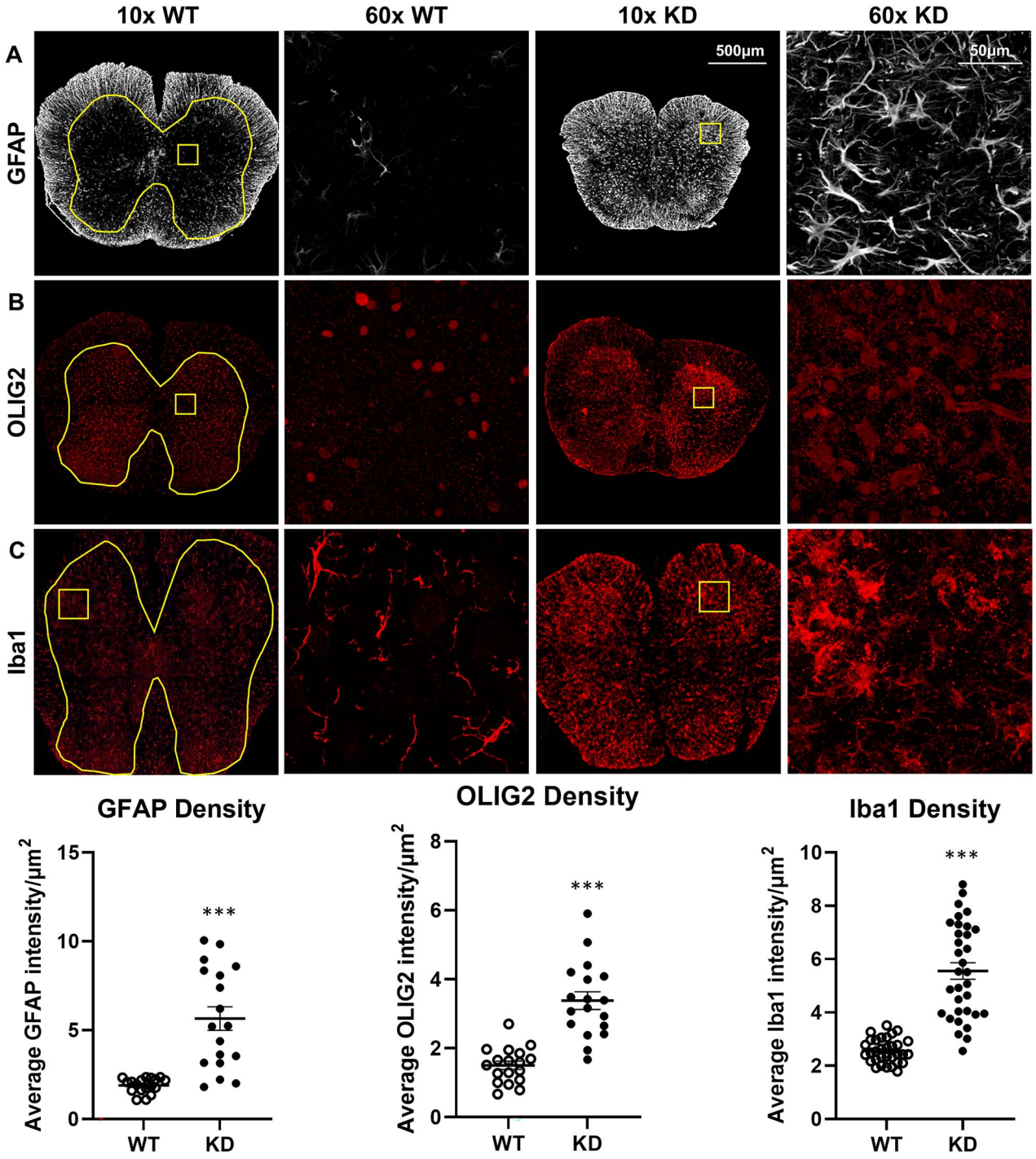

Fig. 4. TDP-43 KD leads to increased GFAP, OLIG2, and Iba1 density in the gray matter of the lumbar spinal cord compared with WT controls. Average density from all quantified images from WT ($N = 5$, $n = 18–32$, 3–7 n per N) and TDP43 KD mice ($N = 6$, $n = 18–33$, 3–7 n per N). Yellow boxes highlight 60× inset images; an example ROI is shown in yellow on WT 10× images. Individual data points are plotted with mean and SEM. Two-tailed unpaired t-test shows significant differences at $P < 0.0001$ (***).

or genetic conditions such as Down syndrome and related early-onset AD; and traumatic CNS injury-related diseases such as chronic traumatic encephalopathy (CTE) (Chornenkyy et al. 2019). Our results suggest that global TDP-43 reduction leads to the neuronal accumulation of dsRNA, and thus it will be interesting to determine if the TDP-43 proteinopathies described above display dsRNA accumulation.

In summary, this study provides novel in vivo evidence that TDP-43 dysfunction leads to dsRNA accumulation in the spinal cords of mice and potentially in the brains of human FTD/ALS patients. Because we were limited to a small number of animals and a small amount of fixed tissue, many questions were out of our reach. Future studies expanding sample sizes and timelines of pathologies could provide additional insight. With an expanded colony of amiR-TDP43 animals and cell-type specific TDP43 KO lines, we could more directly investigate possible sources of dsRNA and establish a timeline for dsRNA deposition, neurodegeneration, and the onset of gliosis. We could expand our previous

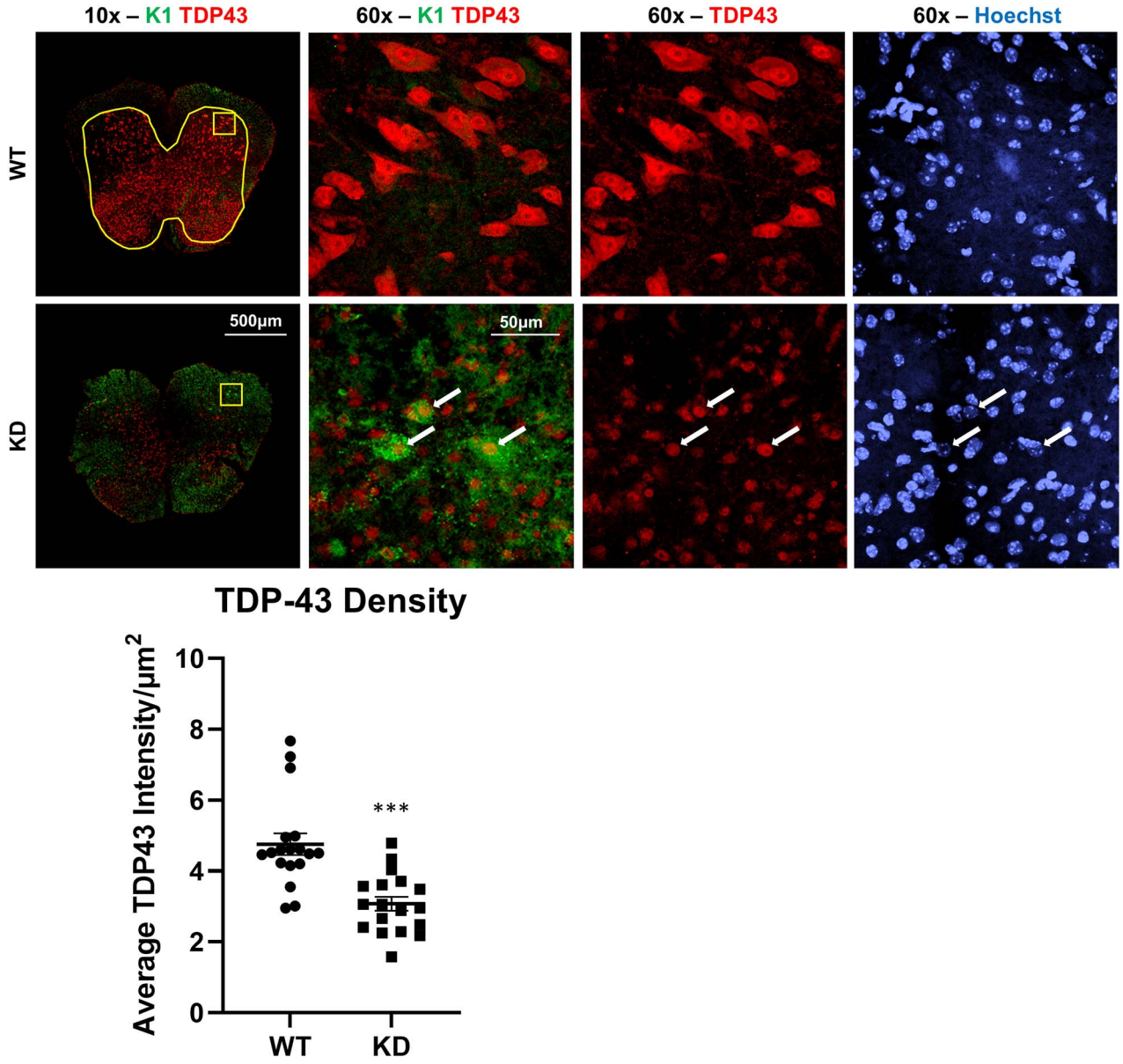

Fig. 5. TDP-43 KD leads to decreased TDP-43 density in the gray matter of the lumbar spinal cord compared with WT controls, especially in regions of high dsRNA. Average density from all quantified images from WT ($N = 6$, $n = 18$, 3 n per N) and TDP43 KD mice ($N = 6$, $n = 18$, 3 n per N). Yellow boxes highlight 60× inset images; an example ROI is shown in yellow on WT 10× images. White arrows indicate Hoechst+/TDP43+ high K1 cells with reduced cytoplasmic TDP-43 staining. Individual data points are plotted with mean and SEM. Two-tailed unpaired t-test shows significant differences at $P < 0.0001$ (***).

Table 1. Age, symptoms, and average staining levels for each animal used in this study.

Mouse	Age (days)	Stage	dsRNA	TDP43	NeuN	GFAP	Iba1
KD 6	53	Paralysis	+	++	++	++	++
KD 16	59	Paralysis Weight loss	++	++	++	++	++
KD 23	49	Right side paralysis Weight loss	+++	+	+	+++	+++
KD 29	26	Paralysis	+++	+	+	+++	+++
KD 38	30	Hindlimb paralysis	+	++	+	+++	+++
KD 55	23	Paralysis	+	++	++	++	++
Avg WT	44.5	None	–	+++	+++	+	+

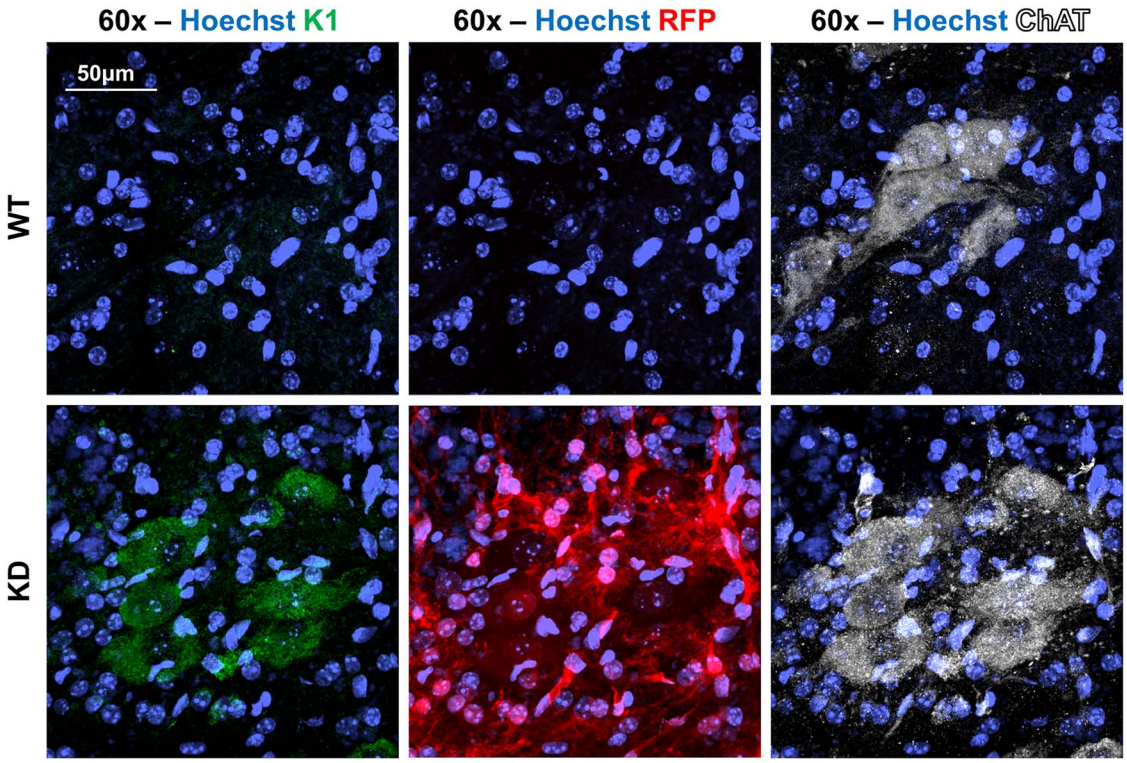

Fig. 6. TDP-43 KD leads to increased dsRNA in motor neurons of the lumbar spinal cord compared with WT controls. TDP43 KD was confirmed via RFP immunostaining, and 60× oil-immersion images were taken from the ventral horn of the lumbar spinal cord. $N = 6$, $n = 18$, 3 n per N for WT, and $N = 6$, $n = 18$, 3 n per N for TDP43 KD.

results to different brain regions that are affected by ALS/FTD and other TDP-43 proteinopathies.

If dsRNA accumulation can be causally linked to the pathologies observed in ALS/FTD, it may represent a novel therapeutic target for these untreatable diseases.

Acknowledgments

We thank Kora Kastengren, Curtis Borski, Joseph Dragavon, and the Advanced Light Microscopy Core Facility at the University of Colorado, Boulder.

Funding

National Institutes of Health (R01 AG064465, NS086933, and NS063964); LeJeune Foundation #1805; Linda Crnic Institute; AB Nexus pilot support funding program (University of Colorado).

Conflict of interest statement: The authors declare no competing financial interests.

References

Amador-Ortiz C, Lin W-L, Ahmed Z, Personett D, Davies P, Duara R, Graff-Radford NR, Hutton ML, Dickson DW. TDP-43 immunoreactivity in hippocampal sclerosis and Alzheimer's disease. *Ann Neurol*. 2007:61(5):435–445. https://doi.org/10.1002/ana.21154.

Buratti E, Baralle FE. Characterization and functional implications of the RNA binding properties of nuclear factor TDP-43, a novel splicing regulator of CFTR exon 9. *J Biol Chem*. 2001:276(39):36337–36343. https://doi.org/10.1074/jbc.M104236200.

Cassiani-Ingoni R, Coksaygan T, Xue H, Reichert-Scrivner SA, Wiendl H, Rao MS, Magnus T. Cytoplasmic translocation of Olig2 in adult glial progenitors marks the generation of reactive astrocytes following autoimmune inflammation. *Exp Neurol*. 2006:201(2):349–358. https://doi.org/10.1016/j.expneurol.2006.04.030.

Chiang P-M, Ling J, Jeong YH, Price DL, Aja SM, Wong PC. Deletion of TDP-43 down-regulates Tbc1d1, a gene linked to obesity, and alters body fat metabolism. *Proc Natl Acad Sci U S A*. 2010:107(37):16320–16324. https://doi.org/10.1073/pnas.1002176107.

Chornenkyy Y, Fardo DW, Nelson PT. Tau and TDP-43 proteinopathies: kindred pathologic cascades and genetic pleiotropy. *Lab Investig*. 2019:99(7):993–1007. https://doi.org/10.1038/s41374-019-0196-y.

Dunker W, Ye X, Zhao Y, Liu L, Richardson A, Karijolich J. TDP-43 prevents endogenous RNAs from triggering a lethal RIG-I-dependent interferon response. *Cell Rep*. 2021:35(2):108976. https://doi.org/10.1016/j.celrep.2021.108976.

Huang S-L, Wu L-S, Lee M, Chang C-W, Cheng W-C, Fang Y-S, Chen Y-R, Cheng P-L, Shen C-KJ. A robust TDP-43 knock-in mouse model of ALS. *Acta Neuropathol Commun*. 2020:8(1):3. https://doi.org/10.1186/s40478-020-0881-5.

Josephs KA, Murray ME, Whitwell JL, Parisi JE, Petrucelli L, Jack CR, Petersen RC, Dickson DW. Staging TDP-43 pathology in Alzheimer's disease. *Acta Neuropathol*. 2014:127(3):441–450. https://doi.org/10.1007/s00401-013-1211-9.

Klim JR, Williams LA, Limone F, Guerra San Juan I, Davis-Dusenbery BN, Mordes DA, Burberry A, Steinbaugh MJ, Gamage KK, Kirchner R et al. ALS-implicated protein TDP-43 sustains levels of STMN2, a mediator of motor neuron growth and repair. *Nat Neurosci*. 2019:22(2):167–179. https://doi.org/10.1038/s41593-018-0300-4.

Kwong LK, Neumann M, Sampathu DM, Lee VM-Y, Trojanowski JQ. TDP-43 proteinopathy: the neuropathology underlying major forms of sporadic and familial frontotemporal lobar degeneration and motor neuron disease. *Acta Neuropathol*. 2007:114(1):63–70. https://doi.org/10.1007/s00401-007-0226-5.

LaRocca TJ, Mariani A, Watkins LR, Link CD. TDP-43 knockdown causes innate immune activation via protein kinase R in astrocytes. *Neurobiol Dis*. 2019:132:104514. https://doi.org/10.1016/j.nbd.2019.104514.

Ling JP, Pletnikova O, Troncoso JC, Wong PC. TDP-43 repression of nonconserved cryptic exons is compromised in ALS-FTD. *Science*. 2015:349(6248):650–655. https://doi.org/10.1126/science.aab0983.

Peng AYT, Agrawal I, Ho WY, Yen Y-C, Pinter AJ, Liu J, Phua QXC, Koh KB, Chang J-C, Sanford E et al. Loss of TDP-43 in astrocytes leads to motor deficits by triggering A1-like reactive phenotype and triglial dysfunction. *Proc Natl Acad Sci*. 2020:117(46):29101–29112. https://doi.org/10.1073/pnas.2007806117.

Rodriguez S, Sahin A, Schrank BR, Al-Lawati H, Costantino I, Benz E, Fard D, Albers AD, Cao L, Gomez AC et al. Genome-encoded cytoplasmic double-stranded RNAs, found in C9ORF72 ALS-FTD brain, propagate neuronal loss. *Sci Transl Med*. 2021:13(601):eaaz4699. https://doi.org/10.1126/scitranslmed.aaz4699.

Saldi TK, Ash PE, Wilson G, Gonzales P, Garrido-Lecca A, Roberts CM, Dostal V, Gendron TF, Stein LD, Blumenthal T et al. TDP-1, the Caenorhabditis elegans ortholog of TDP-43, limits the accumulation of double-stranded RNA. *EMBO J*. 2014:33(24):2947–2966. https://doi.org/10.15252/embj.201488740.

Saldi TK, Gonzales P, Garrido-Lecca A, Dostal V, Roberts CM, Petrucelli L, Link CD. The Caenorhabditis elegans Ortholog of TDP-43 regulates the chromatin localization of the heterochromatin protein 1 homolog HPL-2. *Mol Cell Biol*. 2018:38(15):e00668–e00617. https://doi.org/10.1128/MCB.00668-17.

Schönborn J, Oberstrass J, Breyel E, Tittgen J, Schumacher J, Lukacs N. Monoclonal antibodies to double-stranded RNA as probes of RNA structure in crude nucleic acid extracts. *Nucleic Acids Res*. 1991:19(11):2993–3000.

Shelkovnikova TA, Kukharsky MS, An H, Dimasi P, Alexeeva S, Shabir O, Heath PR, Buchman VL. Protective paraspeckle hyper-assembly downstream of TDP-43 loss of function in amyotrophic lateral sclerosis. *Mol Neurodegener*. 2018:13(1):30. https://doi.org/10.1186/s13024-018-0263-7.

Sreedharan J, Blair IP, Tripathi VB, Hu X, Vance C, Rogelj B, Ackerley S, Durnall JC, Williams KL, Buratti E et al. TDP-43 mutations in familial and sporadic amyotrophic lateral sclerosis. *Science*. 2008:319(5870):1668–1672. https://doi.org/10.1126/science.1154584.

Stribl C, Samara A, Trümbach D, Peis R, Neumann M, Fuchs H, Gailus-Durner V, Hrabě de Angelis M, Rathkolb B, Wolf E et al. Mitochondrial dysfunction and decrease in body weight of a transgenic knock-in mouse model for TDP-43. *J Biol Chem*. 2014:289(15):10769–10784. https://doi.org/10.1074/jbc.M113.515940.

Sun M, Bell W, LaClair KD, Ling JP, Han H, Kageyama Y, Pletnikova O, Troncoso JC, Wong PC, Chen LL. Cryptic exon incorporation occurs in Alzheimer's brain lacking TDP-43 inclusion but exhibiting nuclear clearance of TDP-43. *Acta Neuropathol*. 2017:133(6):923–931. https://doi.org/10.1007/s00401-017-1701-2.

van Blitterswijk M, Landers JE. RNA processing pathways in amyotrophic lateral sclerosis. *Neurogenetics*. 2010:11(3):275–290. https://doi.org/10.1007/s10048-010-0239-4.

Watanabe S, Oiwa K, Murata Y, Komine O, Sobue A, Endo F, Takahashi E, Yamanaka K. ALS-linked TDP-43M337V knock-in mice exhibit splicing deregulation without neurodegeneration. *Mol Brain*. 2020:13(1):8. https://doi.org/10.1186/s13041-020-0550-4.

White MA, Kim E, Duffy A, Adalbert R, Phillips BU, Peters OM, Stephenson J, Yang S, Massenzio F, Lin Z et al. TDP-43 gains function due to perturbed autoregulation in a Tardbp knock-in mouse model of ALS-FTD. *Nat Neurosci*. 2018:21(4):552–563. https://doi.org/10.1038/s41593-018-0113-5.

Woodburn SC, Bollinger JL, Wohleb ES. The semantics of microglia activation: neuroinflammation, homeostasis, and stress. *J Neuroinflammation*. 2021:18(1):258. https://doi.org/10.1186/s12974-021-02309-6.

Yang C, Tan W, Whittle C, Qiu L, Cao L, Akbarian S, Xu Z. The C-terminal TDP-43 fragments have a high aggregation propensity and harm neurons by a dominant-negative mechanism. *PLoS One*. 2010:5(12):e15878. https://doi.org/10.1371/journal.pone.0015878.

Yang C, Qiu L, Xu Z. Specific gene silencing using RNAi in cell culture. *Methods Mol Biol Clifton NJ*. 2011:793:457–477. https://doi.org/10.1007/978-1-61779-328-8_30.

Yang C, Wang H, Qiao T, Yang B, Aliaga L, Qiu L, Tan W, Salameh J, McKenna-Yasek DM, Smith T et al. Partial loss of TDP-43 function causes phenotypes of amyotrophic lateral sclerosis. *Proc Natl Acad Sci U S A*. 2014:111(12):E1121–E1129. https://doi.org/10.1073/pnas.1322641111.

Yousef A, Robinson JL, Irwin DJ, Byrne MD, Kwong LK, Lee EB, Xu Y, Xie SX, Rennert L, Suh E et al. Neuron loss and degeneration in the progression of TDP-43 in frontotemporal lobar degeneration. *Acta Neuropathol Commun*. 2017:5(1):68. https://doi.org/10.1186/s40478-017-0471-3.

Zamanian JL, Xu L, Foo LC, Nouri N, Zhou L, Giffard RG, Barres BA. Genomic analysis of reactive Astrogliosis. *J Neurosci*. 2012:32(18):6391–6410. https://doi.org/10.1523/JNEUROSCI.6221-11.2012.

Zhang Y-J, Guo L, Gonzales PK, Gendron TF, Wu Y, Jansen-West K, O'Raw AD, Pickles SR, Prudencio M, Carlomagno Y et al. Heterochromatin anomalies and double-stranded RNA accumulation underlie *C9orf72* poly(PR) toxicity. *Science*. 2019:363(6428):eaav2606. https://doi.org/10.1126/science.aav2606.